ACS APPLIED MATERIALS & INTERFACES

Research Article

www.acsami.org

# Broad Ranges and Fast Responses of Single-Component Blue-Phase Liquid Crystals Containing Banana-Shaped 1,3,4-Oxadiazole Cores

I-Hung Chiang,[†] Chun-Ji Long,[†] Hsin-Chieh Lin,[†] Wei-Tsung Chuang,[‡] Jey-Jau Lee,[‡] and Hong-Cheu Lin*[,†]

[†]Department of Materials Science and Engineering, National Chiao Tung University, Hsinchu 30049, Taiwan

[‡]National Synchrotron Radiation Research Center, Hsinchu 30076, Taiwan

Supporting Information

**ABSTRACT:** In this study, we synthesized two novel 1,3,4-oxadiazole-based bent-core liquid crystals (**OXD7***, **OXD5B7F***) containing a chiral tail that display broad ranges of the blue phase III (34 and 7 K, respectively); we characterized them using polarized optical microscopy, differential scanning calorimetry, and circular dichroism. The electro-optical responses of both of these liquid crystals are much faster than those of previously reported single-component blue-phase liquid crystals. To optimize its electro-optical performance, we mixed **OXD7*** (the blue-phase range of which is broader than that of **OXD5B7F***) with its analogue **OXD6** (at weight ratios of 6:4 and 4:6). We also performed molecular modeling of single-component BPLCs (**OXD7*** and **OXD5B7F***) to analyze the possible parameters affecting their blue phase ranges.

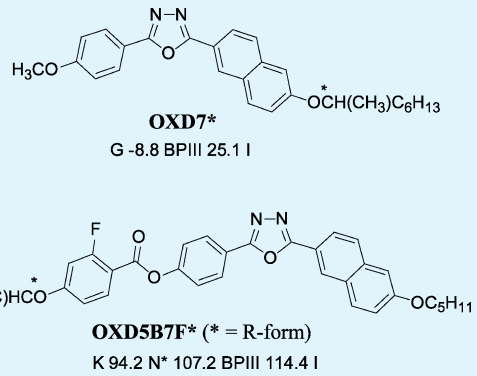


**KEYWORDS:** *bent-core liquid crystal, chiral tail, blue phase III, circular dichroism, single-component blue phase*

## INTRODUCTION

Blue phases (BPs) are liquid crystal (LC) phases normally observed just below the isotropization temperature within a few degrees upon cooling. With the chiral nematic phase induced by the chiral effects of molecular structures, it is possible to form double-twisted cylinders, classified as BPs, in LC materials with high chiralities. According to previous research based on the Kossel diagram method,[1−4] Landau theory,[5−9] electron microscopy, and polarized optical microscopy (POM), BPs can be categorized into three types: BPI, BPII, and BPIII with body-centered cubic, simple cubic, and amorphous symmetric structures, respectively.[11,12] Investigations of BPs for LC display applications have been fruitful in recent years because of, for example, their fast switching times, insensitivity to the cell gap, and alignment layer−free nature.[12] The use of BPs in display applications has, however, been restricted by the narrow temperature ranges of the mesophase, high operating voltages, and $V-T$ hystereses.[13] Accordingly, several methods (e.g., supercooled freezing,[14,15] polymer stabilization,[16,17] nanoparticle stabilization,[18,19] light induction[20,21]) and systems (e.g., bent-core LCs,[22−29] hydrogen-bonded LCs,[30,31] discotic LCs[32,33]) have been employed to extend the BP ranges.[34] Most of these methods to obtain wide BP ranges have, however, required LC mixtures. We suspected that the use of newly developed single-component BPLCs having broad BP ranges would further increase the BP ranges of the whole mixtures. Generally, single-component BPLCs having a range wider than 30 K have all been bent-core LCs;[22−29] and as a result, we focused in this present study on the discovery of novel single-component bent-core BPLCs. Moreover, most of the BPs induced by bent-core LCs have been of type BPIII,[35−38] which display lower degrees of $V-T$ hysteresis relative to types BPI and BPII, due to the amorphous arrangements of the cylinders in BPIII.[38] In addition, because of the amorphous nature, as well as shorter pitch when compared with other BP structures, we expected BPIII types to reflect less visible light in the dark state than would other BPs. Several single-component bent-core (including banana-, T-, and U-shaped) LCs for BP applications have been investigated for their tendency to exhibit biaxial optical activity.[26,39−43] Biaxial helical structures are expected to have greater positive impact on the phases of BPs than would uniaxial helical structures.[41−45] In addition, chirality also plays an important role in BPs.[46,47] Among the tested LCs, the banana-shaped LCs greatly enhanced the effects of the chiral structures as a result of their bent-core nature.[48,49] Banana-shaped LCs featuring oxadiazoles as the central cores have been the most successful units for achieving biaxiality in the nematic phase because their large transversal dipole moments stabilize the biaxial nematic phase.[48,50−52] Moreover, asymmetric structures presenting lateral fluoro substituents can broaden the BP or lower the isotropization temperature.[41,48,53]

**Received:** September 13, 2013
**Accepted:** December 9, 2013
**Published:** December 9, 2013

  

Accordingly, in this study we synthesized two asymmetric 1,3,4-oxadiazole-based bent-core LCs presenting a chiral tail to induce BPs. In a previous study,[54] we had prepared a series of 1,3,4-oxadiazole-based bent-core LCs (OXD*n*), featuring different alkyl chain lengths (*n*), that displayed biaxial properties. For this present investigation, we synthesized **OXD7***, a chiral analogue of OXDn, and **OXD5B7F***, another asymmetric bent-core LC presenting a lateral fluoro substituent containing a chiral tail. Figure 1 reveals that **OXD7*** and **OXD5B7F*** both

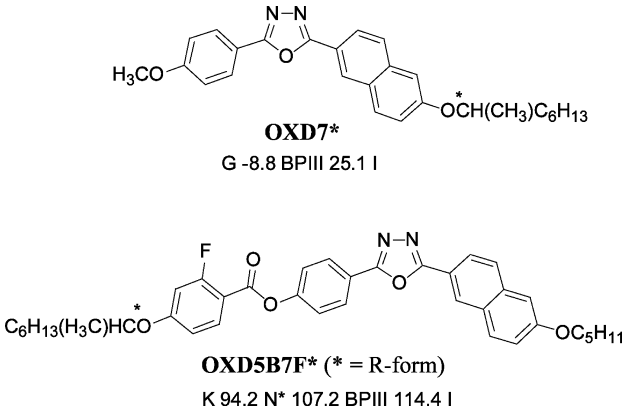


**Figure 1.** Chemical structures and phase transition temperatures (upon the first cooling) of **OXD7*** and **OXD5B7F***; [$\Delta H$/J/g] ($\Delta C_p$/J/g*°C). I: Isotropic liquid crystal state. N*: Cholesteric phase. K: Crystal. G: Glassy state.

demonstrated BPIII temperature ranges: 34 K (at room temperature) and 7 K, respectively. Surprisingly, the electro-optical response times of the single-component BPs of **OXD7*** and **OXD5B7F*** were much faster than those of other reported single-component BPs possessing wide temperature ranges.[26,27]

Although many studies have been made into the stability of BPs in mixtures,[55−59] none have been performed for single-component BPs, possibly because of the scarcity of single-component BPLCs. For this present study, therefore, we investigated several of the features that might stabilize the BPIII forms of **OXD7*** and **OXD5B7F***, including the length-to-width ratio, dipole moment, bending angle, helical twist power (HTP), and molecular conformation.

## EXPERIMENTAL SECTION

**Synthesis.** The single-component BPs of **OXD7*** and **OXD5B7F*** were synthesized according to Schemes 1 and 2; the synthetic details are provided in the Supporting Information. Chemical characterization data of **OXD7*** and **OXD5B7F*** are provided below.

*2-(2-((-[(R)-Octan-2-yloxy)]naphthalen-6-yl)-5-(4-methoxyphenyl)-1,3,4-oxadiazole (**OXD7***).* $^1$H NMR (300 MHz, $CDCl_3$) $\delta$ (ppm): 8.49 (s, 1H), 8.14−8.01 (m, 3H), 7.85−7.70 (m, 2H), 7.25−7.19 (m, 1H), 7.16 (d, $J$ = 4.2 Hz, 1H), 7.02 (d, $J$ = 11.1 Hz, 2H), 4.56−4.50 (m, 1H), 3.88 (s, 3H), 2.15−1.24 (m, 13H), 0.86 (t, $J$ = 6.9 Hz, 3H). $^{13}$C NMR (75 MHz, $CDCl_3$) $\delta$ (ppm): 14.20, 19.71, 22.72, 25.62, 29.38, 31.91, 36.49, 55.54, 74.09, 108.13, 114.57, 116.67, 118.98, 121.02, 123.81, 126.95, 127.67, 128.16, 128.75, 130.49, 136.34, 157.93, 162.36, 164.43, 164.63. Anal. Calcd for $C_{27}H_{30}N_2O_3$: C, 75.32; H, 7.02; N, 6.51. Found: C, 75.18; H, 6.87; N, 6.63.

*4-(5-[2-(Pentyloxy)naphth-6-yl]-1,3,4-oxadiazol-2-yl)phenyl 4-[(R)-octan-2-yloxy]-2-fluorobenzoate (**OXD5B7F***).* $^1$H NMR (300 MHz, $CDCl_3$) $\delta$ (ppm): 8.51 (s, 1H), 8.22−8.10 (m, 2H), 8.03 (t, $J$ = 9.0 Hz, 2H), 7.83 (t, $J$ = 8.7 Hz, 2H), 7.41 (d, $J$ = 6.6 Hz, 2H), 7.24−7.19 (m, 1H), 7.16 (d, $J$ = 7.5 Hz, 1H), 6.77−6.64 (m, 2H), 4.43−4.39 (m, 1H), 4.08 (t, $J$ = 6.6 Hz, 2H), 2.15−1.12 (m, 19H), 0.95−0.85 (m, 6H). $^{13}$C NMR (75 MHz, $CDCl_3$) $\delta$ (ppm): 13.90, 19.31, 22.32, 22.43, 25.19, 28.08, 28.71, 29.02, 31.59, 36.01, 68, 74.79, 103.36, 103.70, 106.44, 108.81, 108.94, 111.51, 118.51, 120.16, 121.4, 122.47, 123.57, 126.91, 127.5, 127.96, 128.06, 130.11, 133.76, 136.17, 153.17, 158.7, 161.77, 161.82, 162.29, 163.62, 164.17, 164.33, 164.82, 165.75. Anal. Calcd for $C_{38}H_{41}FN_2O_5$: C, 73.06; H, 6.61; N, 4.48. Found: C, 73.15; H, 6.64; N, 4.79.

**Characterization.** $^1$H and $^{13}$C NMR spectra were recorded using a Varian Unity 300 MHz spectrometer and $d_6$-DMSO and $CDCl_3$ as solvents. Mass spectra were recorded using a Micromass TRIO-2000 GC-MS instrument. Elemental analyses (EA) were performed using a PerkinElmer 240C elemental analyzer. Mesophasic textures were characterized using a polarized optical microscope (Leica DMLP) equipped with a hot stage (Linkam TMS-94/LTS350). Temperatures and enthalpies of phase transitions were determined through differential scanning calorimetry (DSC) at peak maxima (Perkin Elmer Diamond), with heating rates for **OXD7*** and **OXD5B7F*** of 5 and 1 °C/min, respectively. Circular dichroism (CD) spectra were measured using an AVIV Model 410 apparatus; the samples were placed between two sandwiched pieces of untreated quartz glass. Synchrotron powder X-ray diffraction (XRD) measurements were performed at beamlines BL01C2, 17A1, and 13A1 of the National Synchrotron Radiation Research Center (NSRRC), Taiwan; the wavelengths of the X-rays ranged from 1.0243 to 1.3302 Å. The powder samples were packed into capillary tubes or dropped on an untreated cover glass and then heated with a heat gun, the temperature controller of which was programmable by a computer having a PID feedback system. The scattering angle ($\theta$) was calibrated using a mixture of silver behenate and silicon. The electro-optical properties were determined using a system comprising a He−Ne laser ($\lambda$ = 633 nm; Thorlabs), a digital oscilloscope (Tektronix TDS-3012B), an arbitrary waveform generator (Tektronix AFG 3021), a high-speed power amplifier (Gwinstek), and an optical power meter (Unice 09OPM-20). The laser light that passed through a commercially in-plane switching (IPS) cell (cell gap = 8 $\mu$m; electrode separation = electrode width = 4 $\mu$m) between two crossed polarizers was detected by the optical power meter (see Supporting Information Figure S2a). For electro-optical measurements, the frequency ($f$) of the square waves was approximately 10 Hz for the $V-T$ curves; a wave packet of

**Scheme 1. Synthesis of OXD7***

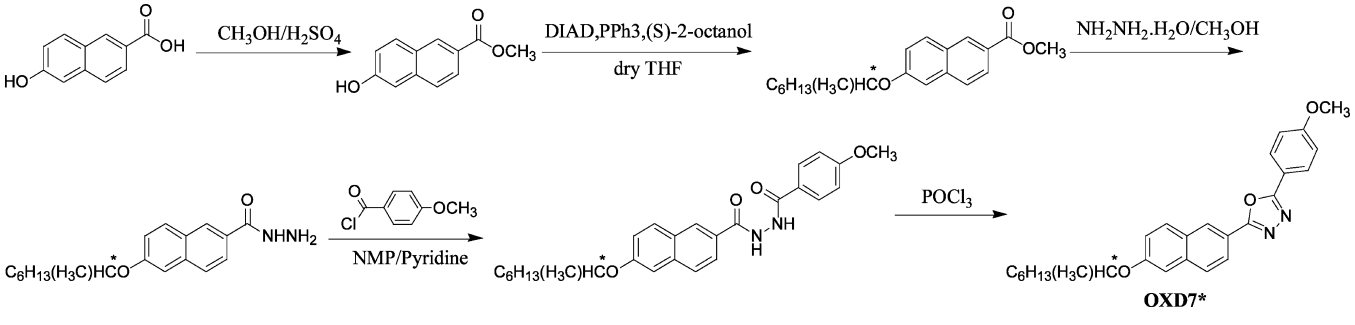



dx.doi.org/10.1021/am403976a | ACS Appl. Mater. Interfaces 2014, 6, 228−235

**Scheme 2. Synthesis of OXD5B7F***

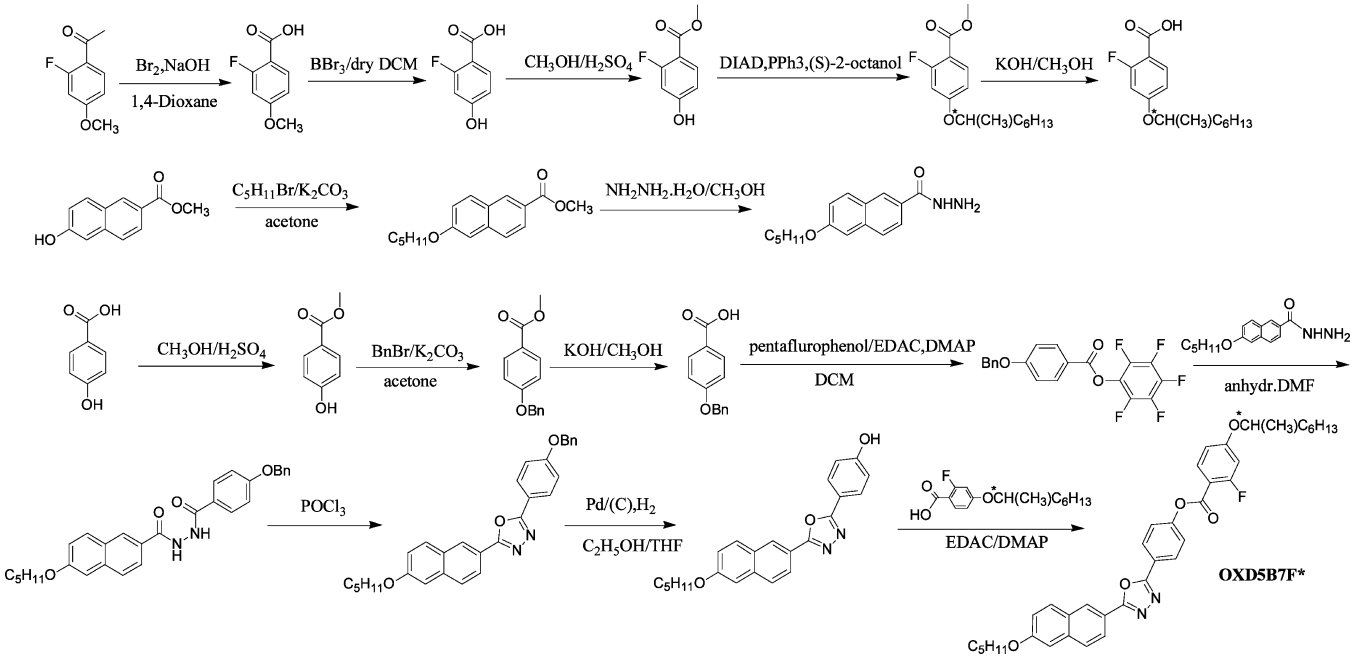


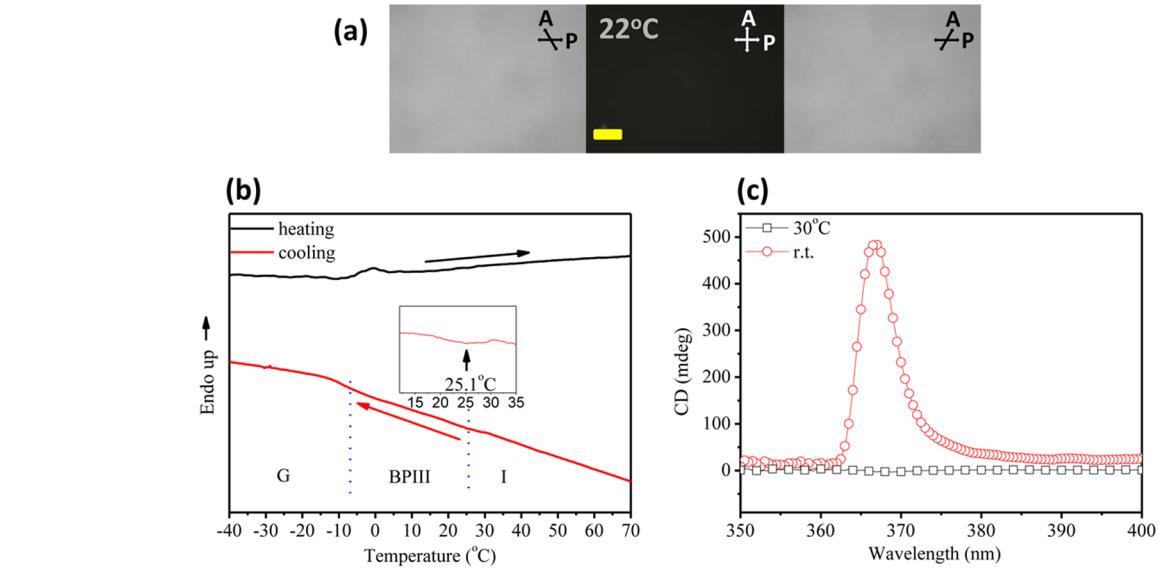


**Figure 2.** (a) POM images (scale bar = 40 $\mu$m), (b) DSC curves (with rate of 5°C/min upon cooling; inset = isotropic-BPIII transition), and (c) CD signals of **OXD7***.

square waves with values of $f$ of approximately 0.7 and 10 Hz (in each wave) was used for measurements of response time values (see Supporting Information Figure S2b). HTP measurements of **OXD7*** and **OXD5B7F*** were preformed using a UV−vis spectrophotometer (Jasco V-670) and wedge cells; the commercial LC JC1041-XX (Chisso) and **OXD5B7F** (an analogue of **OXD5B7F***; see SI for its properties) were used, respectively, as host materials.

## RESULTS AND DISCUSSION

**Mesophasic and Thermal Properties.** We used POM to confirm the existence of the single-component BP for **OXD7***, which possesses both biaxial and chiral properties. Figure 2a (recorded at 22 °C) reveals acentral dark POM image under crossed polarizers and peripheral grey POM images at various angles of the polarizer and analyzer; we attribute these features to the BPIII state, similar to the images of the isotropic state arising from the BPIII form in the UV region. The BPIII state of an LC with high chirality is typically hard to distinguish from the isotropic state because of its (i) isotropic-like nature, (ii) selective reflection peak near the UV region, and (iii) broad signal for the isotropic−BPIII transition during the DSC cooling process.[35] Therefore, we used both DSC and CD measurements (Figures 2b and 2c) to verify the BPIII state of **OXD7***. CD spectroscopy evaluates the differences in absorptions of left- and right-handed circularly polarized light as a function of wavelength; CD signals can appear in chiral systems.[40,60,61] We observed a broad DSC peak (~25.1 °C) for the isotropic−mesophase transition (inset to Figure 2b) and a CD signal with a peak maximum at 367 nm at room temperature (r.t., Figure 2c) for **OXD7*** upon cooling,


dx.doi.org/10.1021/am403976a | ACS Appl. Mater. Interfaces 2014, 6, 228−235

indicating the presence of a chiral phase (possibly an N*, BP, or smectic phase having a chiral structure). The POM images in Figure 2a reveal neither the typical textures of an N* phase (e.g., fingerprint, focal conic, oily-streak, and planar textures) nor the classic mosaic textures of cubic BPs (BPI or BPII).[62,63] In addition, no smectic order was evident in XRD spectra upon cooling **OXD7*** from 50 to 22 °C. Moreover, the $V-T$ curves, as well as the rise and fall times, were similar to reported data for BPIII phases induced by banana-shaped LCs (see the section below describing electro-optical properties). Therefore, the DSC thermogram in Figure 2b revealed that **OXD7*** possessed the BPIII phase upon cooling from +25.1 to −8.8 °C ($T_g$). Similarly, the POM images of **OXD5B7F*** changed from dark (under crossed polarizers) to deep blue at the isotropic−BPIII transition; it turned red at temperatures below 107 °C. After shearing, we observed the typical oily-streak texture of a cholesteric phase. We examined both of these phases with selective reflection by changing the cross angles of the polarizer and analyzer of the polarized optical microscope (Figure 3).

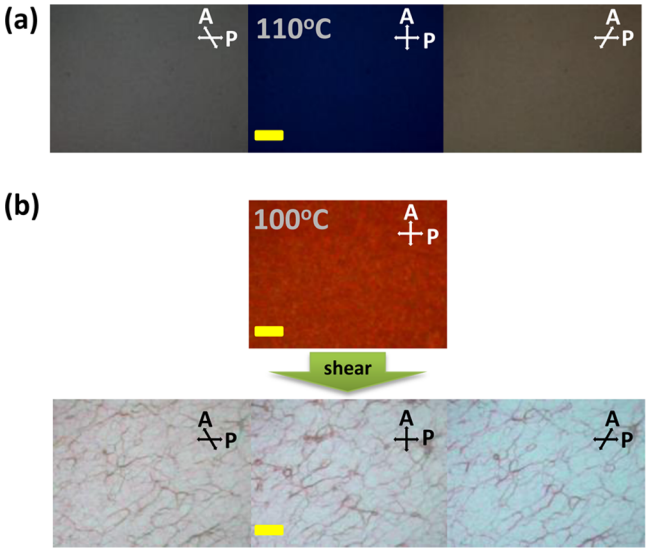


**Figure 3.** POM images of **OXD5B7F*** (scale bar = 40 $\mu$m).

Furthermore, we did not observe any smectic order in the XRD spectra upon cooling from 110 to 103 °C (Figure 4a). As displayed in Figure 4b, we also used DSC to determine the phase transition temperatures of the isotropic−BPIII (114.4 °C) and BPIII−N* (107.2 °C) transitions (inset to Figure 4b). Moreover, most reported compounds possessing a BPIII phase (investigated through DSC during the cooling process) have not exhibited any significant super-cooling effects on the transition of the BPIII;[64−66] we observed similar behavior for **OXD7*** and **OXD5B7F*** (see Figure S3, Supporting Infomation).

We prepared two LC mixtures, **OXD6/OXD7*_6/4** and **OXD6/OXD7*_4/6** (with weight ratios of 6:4 and 4:6, respectively), in an attempt to decrease the driving voltage; their related physical properties are presented below. For **OXD6/OXD7*_4/6**, the POM images were fully dark, even in the BP range, just like those obtained for **OXD7***. Again, we could use DSC and CD to determine the presence of the BPIII phase of **OXD6/OXD7*_4/6**, with a broad DSC peak (~15.7 °C) representing the isotropic−BPIII transition (inset to Figure 5a) and a CD signal appearing below 18 °C (Figure 5b). For **OXD6/OXD7*_6/4**, the POM images changed from dark (under crossed polarizers) to deep blue at the transition from the isotropic state to BPIII at 56 °C (Figure 6a). Below 53 °C, the phase turned to the typical planar texture of a cholesteric phase (Figure 6b). We examined both of these phases with selective reflections by changing the cross angles of the polarizer and the analyzer of the polarized optical microscope. No smectic order was evident from 60 to 40 °C in the XRD spectra (Figure 6c). We could not detect the signal at $T_{I\text{-}BP}$ in the DSC trace (upon cooling), possibly because of its narrow BP range (Figure 6d), but it could still be seen using POM. Table 1 and Figure 7 present the mesophasic properties of all of the tested compounds possessing a BPIII phase. Both **OXD7*** and **OXD6/OXD7*_4/6** feature broad ranges (>25 K) for their BPIII phases at room temperature; **OXD5B7F*** displayed a narrower range for its BPIII phase, but at a higher temperature. In addition, all of our single-component and mixed compounds passed through a monotropic BPIII phase during their cooling cycles.

**Electro-optical Properties.** Figure 8 and Table 2 present the electro-optical properties of the samples, including their $V-T$ curves and switching times, recorded at values of $T-T_{I\text{-}BP}$ of −2 K. To avoid the existence of a mixture between the isotropic and the BP phases, we tested the total response time of **OXD7*** in the BPIII phase not only at 23 °C (~12 ms) but also at 18 °C (~13 ms). This situation arose because of the improvement in the decay times in the BPIII phase: the decay time at 40−30

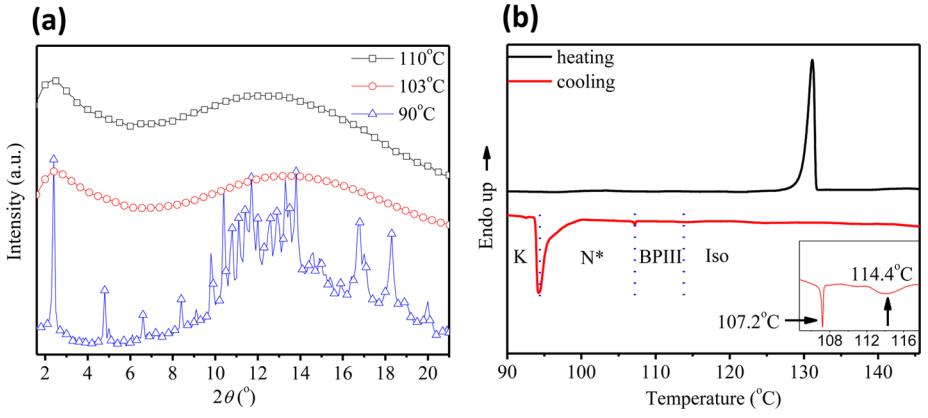


**Figure 4.** (a) XRD spectra recorded at various temperatures (upon cooling) and (b) DSC curves (heating/cooling rate = 1 °C/min; inset shows phase transition peaks) of **OXD5B7F***.


dx.doi.org/10.1021/am403976a | ACS Appl. Mater. Interfaces 2014, 6, 228−235

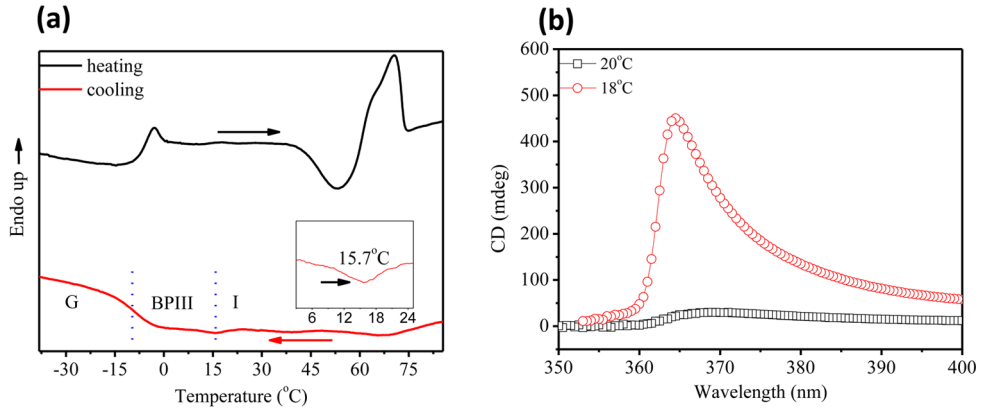


**Figure 5.** (a) CD signals and (b) DSC curves (upon cooling at a rate of 5 °C/min; inset shows isotropic-BPIII transition) of **OXD6/OXD7*_4/6**.

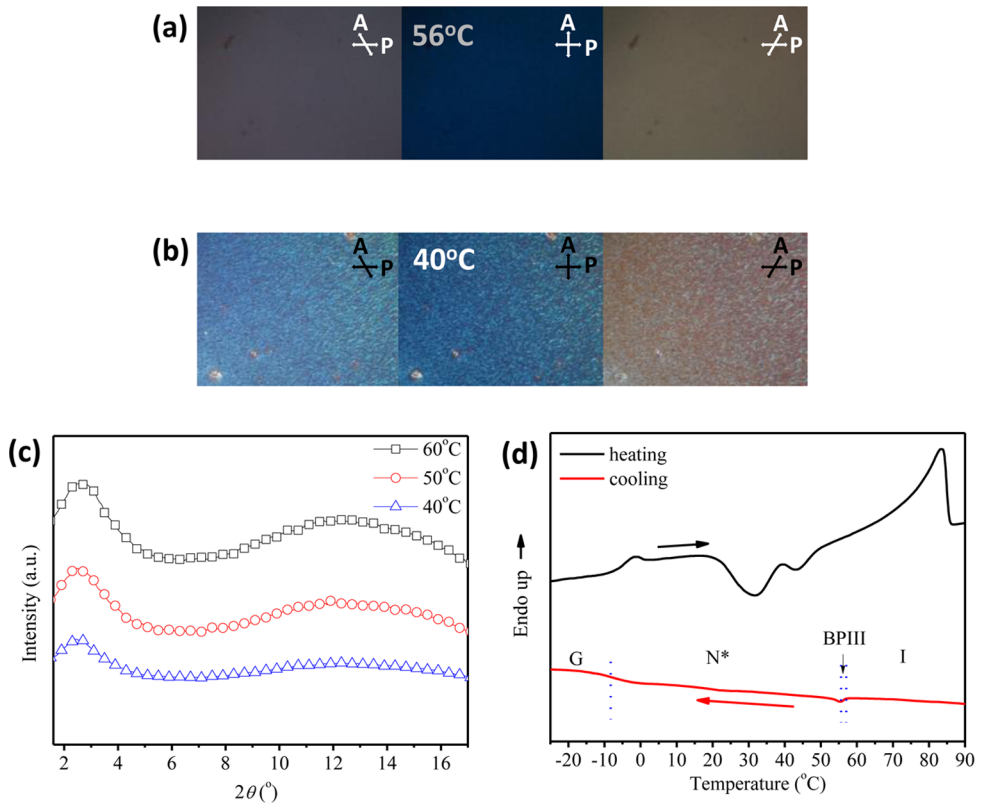


**Figure 6.** (a, b) POM images recorded at 56 and 40°C, respectively, (c) XRD spectra, and (d) DSC curves (upon cooling at a rate of 5 °C/min) of **OXD6/OXD7*_6/4**.

**Table 1. Phase Transition Table of Compounds Featuring the BPIII Phase upon Cooling**

| compound | phase transition temperature at first cooling (°C) [$\Delta H$/J/g] ($\Delta$Cp/J/g*°C) | BPIII range (°C) |
|---|---|---|
| OXD6/OXD7*_6/4[a] | G −9.6(0.38) N* 55.1[−0.65] BPIII 58[c] I | 2.9 |
| OXD6/OXD7*_4/6[a] | G −9.6(0.36) BPIII 15.7[−0.37] I | 25.3 |
| OXD7*[a] | G −8.8(0.42) BPIII 25.1[−0.47] I | 33.9 |
| OXD5B7F*[b] | K 94.2[−56.54] N* 107.2[−0.74] BPIII 114.4[−0.93] I | 7.2 |

[a]5 °C/min. [b]1 °C/min. [c]Not observable using DSC, determined using POM only.

°C (~19 ms) was faster than that at 18 °C (8 ms), but the rise times were independent of the temperature from 40 to 18 °C. This behavior may be due to the Kerr effect dominating in the BPIII phase at 18 and 23 °C; both response times were similar, and much faster, than that in the isotropic state (>25 ms, at 40−30 °C). Therefore, the BPIII and isotropic phases were distinguishable in our case; the lower viscosity of the isotropic state could not improve the switching response further, in contrast to the BPIII state. The $V-T$ curves shifted to the left-hand side upon decreasing the effect of the chiral structure of **OXD7***, either via chemical synthesis of **OXD5B7F*** or the preparation of **OXD6/OXD7*** physical mixtures. They also exhibited no obvious hystereses, as is typical for the $V-T$ curves of BPIII phases.[12,38] The $V-T$ curves show that **OXD5B7F*** displayed the highest maximum light intensity (>5 times) than


dx.doi.org/10.1021/am403976a | ACS Appl. Mater. Interfaces 2014, 6, 228−235

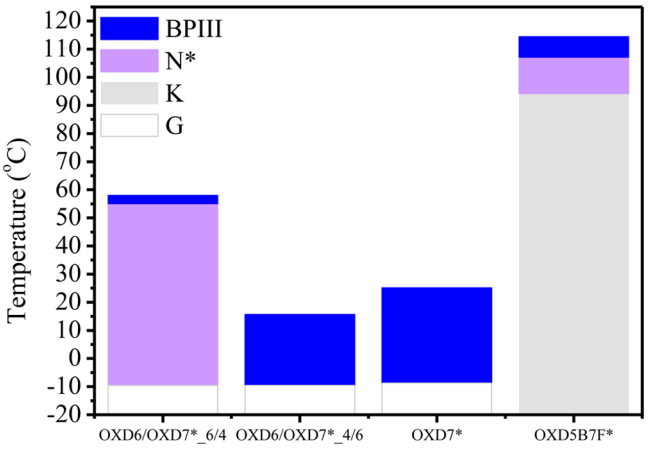


**Figure 7.** Phase diagram of all compounds featuring the BPIII phase (upon cooling).

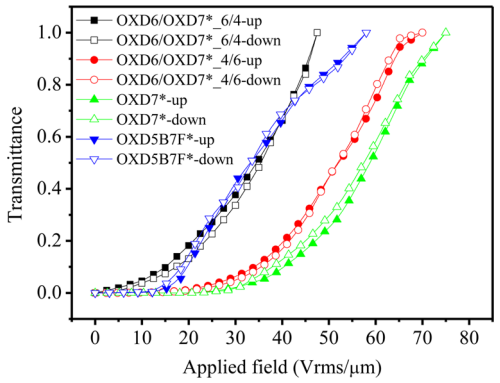


**Figure 8.** $V-T$ curves of all compounds featuring the BPIII phase (at $T-T_{I\text{-}BP} = -2$ K).

**Table 2. Response Time Values of Tested Compounds Featuring the BPIII Phase (at $T-T_{I\text{-}BP} = -2$ K)**

| compound | rise time (ms) | fall time (ms) | total time (ms) |
|---|---|---|---|
| OXD6/OXD7*_6/4 | 2.2 | 5.9 | 8.1 |
| OXD6/OXD7*_4/6 | 3.8 | 5.1 | 8.9 |
| OXD7* | 5.0 | 6.9 | 11.7 |
| OXD5B7F* | 3.1 | 8.7 | 11.8 |

the other compounds in the BP ranges, but the others showed similar maximum light intensities. All the $V-T$ curves functioned in the framework of the Kerr effect. According to previous research,[66] the on-state voltage ($V_{on}$) is proportional to $\kappa^{1/2}\cdot\rho^{-1}$ in the case of similar intrinsic birefringence ($\Delta n$), dielectric anisotropy ($\Delta\varepsilon$), and electrode configurations, where $\kappa$ is the elastic constant and $\rho$ is the pitch of the BPLC. This feature suggests that the thresholdless behavior of **OXD6/OXD7*_6/4** may be due to (i) the low value of $\kappa$ that resulted from its high operating temperature (~60 °C; in comparison, the other two BPLCs were driven below room temperature) and (ii) the large pitch relative to the other two BPLCs with similar conformations (i.e., **OXD7*** and **OXD6/OXD7*_4/6**). The rise and fall times were less than 10 ms, similar to the reported values for BPIII phases induced by banana-shaped LCs;[35,37,45] these values are much faster than those of reported single-component BPs having temperature ranges wider than 30 K.[26,27] It has been suggested that the BPLCs in banana-shaped structures experience less steric hindrance than those in T- or U-shaped molecules, resulting in lower viscosities and faster switching times in banana-shaped BPs.[12,67,68] Furthermore, we find out that the response time values of our BPLCs (in **OXD7*** and **OXD5B7F***) are independent of applied voltages. However, the other reported LCs with BPIII showed reduced switching time values (especially the rise time) by increasing applied voltages.[12,42]

**Molecular Modeling and Influence of Pitch on the Stabilization of Single-Component BPLCs.** Investigations of the stabilization factors for BPs, especially to extend the BP ranges in mixture systems, have boomed recently.[10,55−59] From a study of a series of bent-core 2,5-disubstituted 1,3,4-oxadiazoles mixed with commercial chiral dopants, Yang et al. inferred that a suitable length-to-width ratio ($L/W > 4$), a strong dipole moment, a large bending angle, and a highly twisted conformation were helpful to stabilize BPs.[55] Molecules with flat geometries can possess two distinguishable short axes; Yoshizawa et al. found that the ratio of these two short axes (i.e., molecular biaxiality) was proportional to the BP range in a series of U-shaped 2,3-difluoro-1,4-diphenylbenzene oligomers doped with chiral addictives,[56] where they found that the LC materials with broader BPIII ranges always possess high HTP values, but not necessarily vice versa. Therefore, to analyze the stabilization factors for single-component BPLCs by after chemical doping (i.e., a chiral center introduced to the flexible chain), in this study we examined the most important elements that affect the BP ranges after physical doping (i.e., BPs induced by mixing of chiral addictives to LCs), such as the values of $L/W$ and HTP, dipole moments, and molecular biaxialities, which as had been were determined in those previous reports. Employing a UV−Vis spectrophotometer and wedge cells, we found that the HTPs of **OXD7*** and **OXD5B7F*** were 7.4 (at 23 °C) and 2.1 (at 112 °C), respectively. We optimized the molecular geometries using the semiempirical PM3 method, which provides good estimates of the geometries of organic molecules in their ground states.[69,70] Accordingly, we can could calculate various parameters for each compound as an isolated molecule, such as its dipole moment, bending angle ($\theta$), as well as the three geometrical parameters defined in Figure 9: $L$ (length along the long axis), $W_1$ (width along the short axis normal to the oxadizole plane), and $W_2$ (width along the short axis parallel to the oxadizole plane). Table 3 compares the stabilization parameters (including values of $L/W$ and HTP, dipole moments, and molecular biaxialities) in **OXD7*** and **OXD5B7F***. Both molecules had similar bending angles of 135−136°, typical values of banana-shaped LCs with oxadiazoles as central cores.[48,50−52] The values of $L/W$ of **OXD7*** are only in the range 3.6−5.5; such values are unfavorable for LC phases.[55] In addition, the molecular dipole moment of **OXD7*** is 2.5 D, a value that which might be not be sufficiently large for stabilization of the BPs.[48,50−52] Both parameters (i.e., $L/W$ and molecular dipole moment) had negative effects on the BP range of **OXD7***, in contrast to their effects for **OXD5B7F***. In contrast, the HTP of **OXD7*** (7.4) was larger than that of **OXD5B7F*** (2.1), indicating that **OXD7*** possesses a stronger twisting effect on its chiral structure due to the larger HTP value. In addition, the molecular biaxiality of **OXD7*** ($W_1/W_2 = 1.5$) is larger than that of **OXD5B7F*** ($W_1/W_2 = 1.0$), meaning that **OXD7***, with its two dissimilar short axes, behaves more like a biaxial molecule.[56] Therefore, even with its insufficient values of $L/W$ and dipole moment, the BPIII phase of **OXD7*** can still be stabilized as a result of its high HTP and distinguishable


dx.doi.org/10.1021/am403976a | ACS Appl. Mater. Interfaces 2014, 6, 228−235

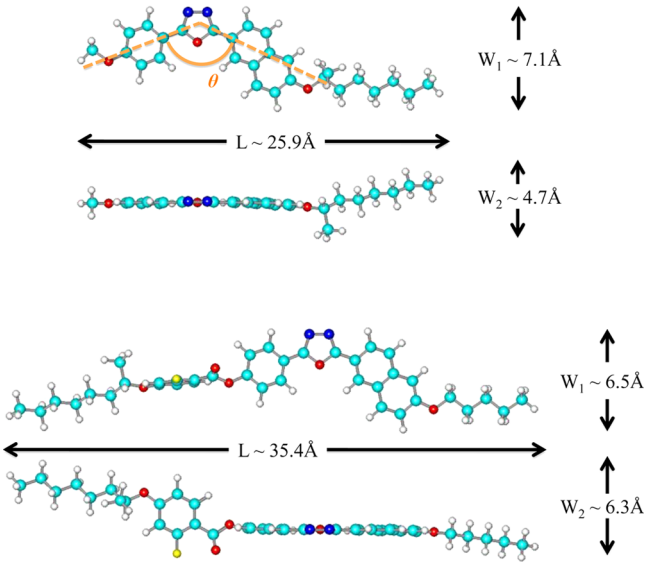


**Figure 9.** Molecular models (simulated using PM3) of the lowest energy conformations of single molecules of (a) **OXD7*** and (b) **OXD5B7F***.

**Table 3. Stabilization Parameters of OXD7* and OXD5B7F***

| compound | bent angle (deg) | dipole moment (debye, D) | $L/W_1$ | $L/W_2$ | $W_1/W_2$ | HTP ($\mu m^{-1}$) |
|---|---|---|---|---|---|---|
| OXD7* | 135.05 | 2.52 | 3.63 | 5.47 | 1.51 | 7.4 |
| OXD5B7F* | 136.56 | 4.73 | 5.41 | 5.62 | 1.04 | 2.1 |

molecular biaxiality, reaching a range of 34 K. On the other hand, regardless of its lower molecular biaxiality and HTP, **OXD5B7F*** can still display a BPIII range of 7 K because of its higher values of $L/W$ and dipole moment. Some previous experimental results[56,59] were focused on the extension of total BP mesophasic ranges, including BPI, BPII, and BPIII. Regardless of the experimental results or computer simulations, if we consider the relationship between BPIII ranges and HTP values in the following references, we can find that the LC materials with broader BPIII ranges always possess high HTP values, but not necessarily vice versa. Our results reveal that the HTP, the molecular biaxiality, the values of $L/W$, and the dipole moment can all help to extend the BP range;[55−59] among them, the HTP and the molecular biaxiality are the two most important factors stabilizing the BPIII phase.

## CONCLUSIONS

The introduction of a chiral center to the soft chain of asymmetrical 1,3,4-oxadiazole-based banana-shaped LCs induces the single-component BPIII phase (with ranges of 34 and 7 K for **OXD7*** and **OXD5B7F***, respectively). To the best of our knowledge, compared with all other reported single-component BPLCs, **OXD7*** exhibits not only the broadest BPIII range (34 K) but also much faster switching (<12 ms) that is independent of the applied voltage. In addition, we have found that the HTPs (measured) and molecular biaxialities (calculated) play important roles in determining the BP ranges of these single-component BPLC systems. Finally, the electro-optical performance, in terms of broader ranges of the BPIII phase at room temperature, could be enhanced further by mixing **OXD7*** with **OXD6**. Although the BP phases of all our reported compounds are only monotropic (they did not crystallize upon annealing), their optimal electro-optical performance (with broader room-temperature ranges of BPIII) might also be enhanced, for the future applications, by mixing them with other compounds featuring enantiotropic BPs. Thus, this study offers possible approaches for the use of **OXD7*** and **OXD5B7F*** either as hosts diluted with nematic LCs to improve electro-optical properties or as chiral dopants (with BPIII) mixed with reported BPLCs possessing good electro-optical properties, thereby extending the BP ranges.

## ASSOCIATED CONTENT

### Supporting Information

Synthesis, properties of **OXD5B7F**, set-up of the optical-electrical and response time measurements, DSC curves upon cooling of **OXD7*** and **OXD5B7F*** at different rates, and mass spectra. This information is available free of charge via the Internet at http://pubs.acs.org/.

## AUTHOR INFORMATION

### Corresponding Author

* Tel: 8863-5712121, ext. 55305. Fax: 8863-5724727. E-mail: linhc@mail.nctu.edu.tw.

### Notes

The authors declare no competing financial interest.

## ACKNOWLEDGMENTS

Financial support of this project was provided by the National Science Council of Taiwan (ROC) through NSC 99-2113-M-009-006-MY2. We thank Drs. Hwo-Shuenn Sheu, Ming-Tao Lee, and Yi-Hung Lin for assistance with the XRD and CD measurements at BL01C2, 17A1, 13A1, and 04B1 at the National Synchrotron Radiation Research Center (NSRRC) in Taiwan.

## REFERENCES

(1) Cladis, P. E.; Garel, T.; Pieranski, P. *Phys. Rev. Lett.* **1986**, *57*, 2841−2844.
(2) Jérôme, B.; Pieranski, P. *Liq. Cryst.* **1989**, *5*, 799−812.
(3) Miller, R. J.; Gleeson, H. F.; Lydon, J. E. *Phys. Rev. Lett.* **1996**, *77*, 857−860.
(4) Kossel, W.; Loeck, V.; Voges, H. *Z. Phys. A: Hadrons Nucl.* **1935**, *94*, 139.
(5) Hornreich, R. M.; Shtrikman, S. *Phys. Rev. A* **1981**, *24*, 635−638.
(6) Kleinert, H.; Maki, K. *Fortschr. Phys.* **1981**, *29*, 219−259.
(7) Grebel, H.; Hornreich, R. M.; Shtrikman, S. *Phys. Rev. A* **1984**, *30*, 3264−3278.
(8) Belyakov, V A; Dmitrienko, V. E *Phys.—Usp.* **1985**, *28*, 535−562.
(9) Longa, L.; Monselesan, D.; Trebin, H.-R. *Liq. Cryst.* **1989**, *5*, 889−898.
(10) Coles, H. J.; Pivnenko, M. N. *Nature* **2005**, *436*, 997−1000.
(11) Kikuchi, H. *Struct. Bonding* **2008**, *128*, 99−117.
(12) Yoshizawa, A.; Kamiyama, M.; Hirose, T. *Appl. Phys. Express* **2011**, *4*, No. 101701.
(13) Rao, L.; Yan, J.; Wu, S. T.; Yamamoto, S.; Haseba, Y. *Appl. Phys. Lett.* **2011**, *98*, No. 081109.
(14) Zhang, B. Y.; Meng, F. B.; Cong, Y. H. *Opt. Express* **2007**, *15*, 10175−10181.
(15) Gilli, J. M.; Kamaye, M.; Sixou, P. *Mol. Cryst. Liq. Cryst.* **1991**, *199*, 79−86.
(16) Kikuchi, H.; Yokota, M.; Hisakado, Y.; Yang, H.; Kajiyama, T. *Nat. Mater.* **2002**, *1*, 64−68.
(17) Iwata, T.; Suzuki, K.; Amaya, N.; Higuchi, H.; Masunaga, H.; Sasaki, S.; Kikuchi, H. *Macromolecules* **2009**, *42*, 2002−2008.

(18) Yoshida, H.; Tanaka, Y.; Kawamoto, K.; Kubo, H.; Tsuda, T.; Fujii, A.; Kuwabata, S.; Kikuchi, H.; Ozaki, M. *Appl. Phys. Express* **2009**, *2*, No. 121501.
(19) Karatairi, E.; Rozic, B.; Kutnjak, Z.; Tzitzios, V.; Nounesis, G.; Cordoyiannis, G.; Thoen, J.; Glorieux, C.; Kralj, S. *Phys. Rev. E* **2010**, *81*, No. 041703.
(20) Chanishvili, A.; Chilaya, G.; Petriashvili, G.; Collings, P. J. *Phys. Rev. E* **2005**, *71*, No. 51705.
(21) Liu, H. Y.; Wang, C. T.; Hsu, C. Y.; Lin, T. H.; Liu, J. H. *Appl. Phys. Lett.* **2010**, *96*, No. 121103.
(22) Yoshizawa, A. *J. Soc. Inf. Disp.* **2008**, *16*, 1189−1194.
(23) Iwamochi, H.; Yoshizawa, A. *Mol. Cryst. Liq. Cryst.* **2009**, *509*, 223−232.
(24) Nakata, M.; Takanishi, Y.; Watanabe, J.; Takezoe, H. *Phys. Rev. E* **2003**, *68*, No. 41710.
(25) Zheng, Z.; Shen, D.; Huang, P. *New J. Phys.* **2010**, *12*, No. 113018.
(26) Yoshizawa, A.; Kogawa, Y.; Kobayashi, K.; Takanishi, Y.; Yamamoto, J. *J. Mater. Chem.* **2009**, *19*, 5759−5764.
(27) Iwamochi, H.; Hirose, T.; Kogawa, Y.; Yoshizawa, A. *Chem. Lett.* **2010**, *39*, 170−171.
(28) Wang, L.; He, W.; Xiao, X.; Yang, Q.; Yang, B.; Li, P.; Yang, H. *J. Mater. Chem.* **2012**, *22*, 2383−2386.
(29) Park, K.-W.; Gim, M.-J.; Kim, S.; Hur, S.-T.; Choi, S.-W. *ACS Appl. Mater. Interfaces* **2013**, *5*, 8025−8029.
(30) He, W. L.; Pan, G. H.; Yang, Z.; Zhao, D. Y.; Niu, G. G.; Huang, W.; Yuan, X. T.; Guo, J. B.; Cao, H.; Yang, H. *Adv. Mater.* **2009**, *21*, 2050−2053.
(31) Ely, F.; Conte, G.; Merlo, A.; Gallardo, H. *Liq. Cryst.* **2004**, *31*, 1413−1425.
(32) Hauser, A.; Thieme, M.; Saupe, A.; Heppke, G.; Krüerke, D. *J. Mater. Chem.* **1997**, *7*, 2223−2229.
(33) Krüerke, D.; Kitzerow, H. S.; Heppke, G.; Vill, V. *Ber. Bunsen-Ges.* **1993**, *97*, 1371−1375.
(34) He, W.; Wang, L.; Wang, L.; Cui, X.; Xie, M.; Yang, H. *Prog. Chem.* **2012**, *24*, 182−192.
(35) Taushanoff, S.; Le, K. V.; Williams, J.; Twieg, R. J.; Sadashiva, B. K.; Takezoe, H.; Jakli, A. *J. Mater. Chem.* **2010**, *20*, 5893−5898.
(36) Lee, M.; Hur, S. T.; Higuchi, H.; Song, K.; Choi, S-W; Kikuchi, H. *J. Mater. Chem.* **2010**, *20*, 5813−5816.
(37) Le, K. V.; Aya, S.; Sasaki, Y.; Choi, H.; Araoka, F.; Ema, K.; Mieczkowski, J.; Jakli, A.; Ishikawa, K.; Takezoe, H. *J. Mater. Chem.* **2011**, *21*, 2855−2857.
(38) Kogawa, Y.; Hirose, T.; Yoshizawa, A. *J. Mater. Chem.* **2011**, *21*, 19132−19137.
(39) Yelamaggad, C. V.; Bonde, N. L.; Achalkumar, A. S.; Rao, D. S. S.; Prasad, S. K.; Prajapati, A. K. *Chem. Mater.* **2007**, *19*, 2463−2472.
(40) Yelamaggad, C. V.; Shashikala, I. S.; Liao, G.; Rao, D. S. S.; Prasad, S. K.; Li, Q.; Jakli, A. *Chem. Mater.* **2006**, *18*, 6100−6102.
(41) Yoshizawa, A.; Sato, M.; Rokunohe, J. *J. Mater. Chem.* **2005**, *15*, 3285−3290.
(42) Sato, M.; Yoshizawa, A. *Adv. Mater.* **2007**, *19*, 4145−4148.
(43) Yoshizawa, A. *J. Mater. Chem.* **2008**, *18*, 2877−2889.
(44) Wright, D. C.; Mermin, N. D. *Rev. Mod. Phys.* **1989**, *61*, 385−432.
(45) Yoshizawa, A. *Mol. Cryst. Liq. Cryst.* **2010**, *516*, 99−106.
(46) Grebel, H.; Hornreich, R. M.; Shtrikman, S. *Phys. Rev. A* **1983**, *28*, 1114−1138.
(47) Belyakov, V. A.; Demikhov, E. I.; Dmitrienko, V. E.; Dolganov, V. K. *J. Exp. Theor. Phys.* **1985**, *62*, 1173−1182.
(48) Tschierske, C.; Photinos, D. J. *J. Mater. Chem.* **2010**, *20*, 4263−4294.
(49) Thisayukta, J.; Niwano, H.; Takezoe, H.; Watanabe, J. *J. Am. Chem. Soc.* **2002**, *124*, 3354−3358.
(50) Madsen, L. A.; Dingemans, T. J.; Nakata, M.; Samulski, E. T. *Phys. Rev. Lett.* **2004**, *92*, No. 145505.
(51) Bates, M. A. *Chem. Phys. Lett.* **2007**, *437*, 189−192.
(52) Luckhurst, G. R. *Angew. Chem. Int. Ed.* **2005**, *44*, 2834−2836.
(53) Li, B.; He, W.; Wang, L.; Xiao, X.; Yang, H. *Soft Matter* **2013**, *9*, 1172−1177.
(54) Sung, H. H.; Lin, H. C. *Liq. Cryst.* **2004**, *31*, 831−840.
(55) Wang, L.; He, W.; Wang, M.; Wei, M.; Sun, J.; Chen, X.; Yang, H. *Liq. Cryst.* **2013**, *40*, 354−367.
(56) Tanaka, M.; Yoshizawa, A. *J. Mater. Chem. C* **2013**, *1*, 315−320.
(57) Alexander, G. P.; Yeomans, J. M. *Phys. Rev. E: Stat., Nonlinear, Soft Matter Phys.* **2006**, *74*, No. 061706.
(58) Fukuda, J. *Phys. Rev. E: Stat., Nonlinear, Soft Matter Phys.* **2012**, *85*, No. 020701.
(59) Jeong, H.-C.; Aya, S.; Kang, S.; Araoka, F.; Ishikawa, K.; Takezoe, H. *Liq. Cryst.* **2013**, *40*, 951−958.
(60) Paik, P.; Gedanken, A.; Mastai, Y. *ACS Appl. Mater. Interfaces* **2009**, *1*, 1834−1842.
(61) Yonamine, Y.; Yoshimatsu, K.; Lee, S. H.; Hoshino, Yu; Okahata, Y.; Shea, K. J. *ACS Appl. Mater. Interfaces* **2013**, *5*, 374−379.
(62) Picot, O. T.; Dai, M.; Broer, D. J.; Peijs, T.; Bastiaansen, C. W. M. *ACS Appl. Mater. Interfaces* **2013**, *5*, 7117−7121.
(63) Giese, M.; Witt, J. C. D.; Shopsowitz, K. E.; Manning, A. P.; Dong, R. Y.; Michal, C. A.; Hamad, W. Y.; MacLachlan, M. J. *ACS Appl. Mater. Interfaces* **2013**, *5*, 6854−6859.
(64) Singh, U. *Eur. J. Phys.* **2007**, *28*, 113−116.
(65) Dierking, I.; Blenkhorn, W.; Credland, E.; Drake, W.; Kociuruba, R.; Kayser, B.; Michael, T. *Soft Matter* **2012**, *8*, 4355−4362.
(66) Wang, L.; He, W.; Xiao, X.; Wang, M.; Wang, M.; Yang, P.; Zhou, Z.; Yang, H.; Yu, H.; Lu, Y. *J. Mater. Chem.* **2012**, *22*, 19629−19633.
(67) Kang, W. S.; Moon, J. W.; Lee, G. D.; Lee, S. H.; Lee, J. H.; Kim, B. K.; Choi, H. C. *J. Opt. Soc. Korea* **2011**, *15*, 161−167.
(68) Choi, S. S.; Castles, F.; Morris, S. M.; Coles, H. J. *Appl. Phys. Lett.* **2009**, *95*, No. 193502.
(69) Stewart, J. J. P. *J. Comput. Chem.* **1991**, *12*, 320−341.
(70) Kadkina, O. N.; Han, H.; Galyametdinov, Y. G. *J. Organomet. Chem.* **2007**, *692*, 5571−5582.